Current-horn suppression for reduced coherent-synchrotron-radiation-induced emittance growth in strong bunch compression

T. K. Charles,[1,2] D. M. Paganin,[1] A. Latina,[3] M. J. Boland,[2,4] and R. T. Dowd[1,2]

[1]*School of Physics and Astronomy, Monash University, Clayton 3800, Victoria, Australia*
[2]*Australian Synchrotron, 800 Blackburn Road, Clayton 3168, Victoria, Australia*
[3]*European Organization for Nuclear Research (CERN), CH-1211 Geneva 23, Switzerland*
[4]*School of Physics, University of Melbourne, Parkville 3010, Victoria, Australia*

(Received 1 November 2016; published 31 March 2017)

Control of coherent synchrotron radiation (CSR)-induced emittance growth is essential in linear accelerators designed to deliver very high brightness electron beams. Extreme current values at the head and tail of the electron bunch, resulting from strong bunch compression, are responsible for large CSR production leading to significant transverse projected emittance growth. The Linac Coherent Light Source (LCLS) truncates the head and tail current spikes which greatly improves free electron laser (FEL) performance. Here we consider the underlying dynamics that lead to formation of current spikes (also referred to as current horns), which has been identified as caustics forming in electron trajectories. We present a method to analytically determine conditions required to avoid the caustic formation and therefore prevent the current spikes from forming. These required conditions can be easily met, without increasing the transverse slice emittance, through inclusion of an octupole magnet in the middle of a bunch compressor.

DOI: 10.1103/PhysRevAccelBeams.20.030705

I. INTRODUCTION

Recent advances in free electron laser (FEL) facilities have seen the peak brightness increase by several orders of magnitude. With ultrafast pulse durations of 100 fs down to <10 fs, these FELs are capable of imaging structure at the molecular- and atomic-size level and investigating dynamical processes over timescales on the order of femtoseconds [1–4]. Continual demand for high brightness and even shorter pulse durations, places stringent requirements on the electron beam quality and heightened awareness of the role coherent synchrotron radiation (CSR) plays in degrading beam quality [5,6]. This demand for high beam quality is echoed by the linear collider community [7].

For a high-brightness FEL, large peak currents need to be achieved through compressing the electron bunch. This is typically achieved through multistage bunch compression via 4-dipole chicanes. Second-order effects (relating to the energy chirp and second order longitudinal dispersion) that greatly limit compression are usually tackled with the addition of a harmonic cavity [8]. Less commonly optical linearization is used [9,10]. Despite these measures, higher-order terms in the energy chirp introduced by collective effects such as longitudinal wakefields can result in the double-horned current profile structure common found with strong bunch compression [11–16].

These current horns are problematic for a number of important reasons including: creating difficulty in matching beam optics, limiting the degree of compression, and increasing wakefield-induced energy spread [11,17]. However, perhaps the most severe consequence of the current horns is the enhanced CSR produced by the large current excursions, resulting in CSR-induced emittance growth [18–20].

CSR can cause time-dependent transverse kicks, resulting in a centroid offset of different regions (slices) of the bunch [21]. As a result the slice emittance can remain largely unchanged, while the lateral displacement of the slices along the bunch results in a smearing of the transverse phase space and enlargement of the projected emittance. Whilst it is the slice emittance that is often considered of primary importance in the FEL lasing process (as particles only interact within a certain *cooperation length* [22]), the projected emittance is also an important factor being responsible for the beam brightness [11,23,24].

A more uniform current pulse improves FEL performance immensely through increased pulse energy, increased peak power, and greater control over the spectral bandwidth [17,22]. This improvement has been verified experimentally at the Linac Coherent Light Source (LCLS) [17], where collimating the head and tail of the bunch successfully limits CSR-induced emittance growth and improves FEL performance, at the cost of removing 40% of the bunch charge [17,25].

The alternate method we present in this paper, establishes the conditions needed to ensure the current horns cannot form, without the need to collimate. This is done through manipulating the longitudinal phase space in the low energy bunch compressor to inhibit the particle trajectory caustics from forming, which would otherwise result in the double horn current profile.

Several solutions to mitigating the CSR-induced projected emittance growth have been reported [5,26,27]. We address the problem through consideration of these current horns as a caustic phenomenon and present analysis that reveals conditions under which the caustics will not form.

In a recent paper, caustic formation in particle trajectories was identified as being directly associated with current horns in strong bunch compression [28]. The relevant theory relating to caustics and bunch compression will be briefly reviewed in Sec. II, with conditions for the formation of caustic-induced current horns being developed in Sec. III. In Sec. IV we determine the condition required to unfold these caustics and prevent the current horns from forming. This is done through careful control of the second- and third-order longitudinal dispersion, denoted as T_{566} and U_{5666} respectively. In Sec. V a two-stage compression scheme is designed to avoid the caustic formation of current horns, through the addition of an octupole and sextupole to the center of two chicanes. Sextupoles have also been shown experimentally to be capable of controlling and manipulating T_{566} [29–31], and have been suggested as a possible technique for linearizing the longitudinal phase space for bunch compression [9,10]. In a similar manner, here we suggest octupoles are required to vary U_{5666} independently of the first-order longitudinal dispersion, R_{56}. Section VI A details the results of a 6-D tracking simulation of an X-band FEL utilizing the caustic-avoidance techniques presented in Sec. V. Section VI B shows the results of the same technique applied to an S-band linac, where the effects of wakefields are not as strong. These simulations were created using particle-tracking computer simulations calculated using the "Electron Generation and Tracking" (ELEGANT) software toolkit [32]. We give a brief discussion in Sec. VII, and offer some concluding remarks in Sec. VIII.

II. BACKGROUND THEORY: BUNCH COMPRESSION

To longitudinally compress a bunch, an energy chirp correlated with longitudinal position, z_i, is established before the bunch passes through a dispersive region. The path length through though the chicane is variable with energy, and therefore the chirped bunch can be compressed. The energy chirp correlated with z_i is usually established by the rf voltage and phase of the accelerating section and harmonic cavity upstream of the compressor. This creates a relative energy deviation of any particle with respect to the reference particle, expanded to third-order in z_i to be,

$$\delta = \delta_i \frac{E_{i,0}}{E_{f,0}} + h_1 z_i + h_2 z_i^2 + h_3 z_i^3 + O(z_i^4) \tag{1}$$

where z_i is defined as the position from the center of the bunch, $E_{i,0}$ and $E_{f,0}$ are the central energy before and after acceleration respectively, and δ_i is the initial uncorrelated energy spread. The first-, second-, and third-order energy chirps, denoted as h_1, h_2, and h_3 respectively, can be written out as,

$$h_1 = \frac{-k_s V_0 \sin\phi_0 - k_x V_1 \sin\phi_1}{E_0}, \tag{2}$$

$$h_2 = \frac{-k_s^2 V_0 \cos\phi_0 - k_x^2 V_1 \cos\phi_1}{2E_0} \tag{3}$$

and

$$h_3 = \frac{k_s^3 V_0 \sin\phi_0 + k_x^3 V_1 \sin\phi_1}{6E_0} \tag{4}$$

where V_0 and V_1 represent the voltages of the main accelerating section and additional harmonic cavity for linearization [8], k_x and k_s are the wave number of the X-band and S-band rf frequencies used, and ϕ_0 and ϕ_1 are the rf phases of these sections. The rf phase is defined to be zero at the crest of the rf, and the interval $-90° < \phi < 0$ defines the negative slope of the rf curve (where the head of the bunch is accelerated less than the tail).

After passing through the chicane, the final longitudinal position relative to the center of the bunch of any electron is,

$$z_f = z_i + R_{56}\delta + T_{566}\delta^2 + U_{5666}\delta^3 + \cdots \tag{5}$$

where R_{56}, T_{566}, and U_{5666} are the first-, second-, and third-order longitudinal dispersion respectively. Here we ignore the geometric terms as chromatic terms will dominate the transformation for beams with small transverse emittance and large energy spread [33], which is typically the case in FEL bunch compressors.

Equations (1) and (5) together give,

$$z_f = (1 + R_{56})z_i + (h_2 R_{56} + h_1 T_{566})z_i^2 + (2h_1 h_2 T_{566} + h_1^3 U_{5666} + h_3 R_{56})z_i^3 + O(z_i^4). \tag{6}$$

The coefficients of the second and third order terms can be forced to equal zero, to ensure a linear transformation, through adjusting the properties of a harmonic cavity [8,34] or through optical elements which has been considered through analytical and numerical investigations in [10,35,36]. The concept of varying T_{566} through manipulation of the longitudinal phase space via sextupole magnets in dispersive regions, has been investigated analytically in [30,33,37], and shown experimentally in

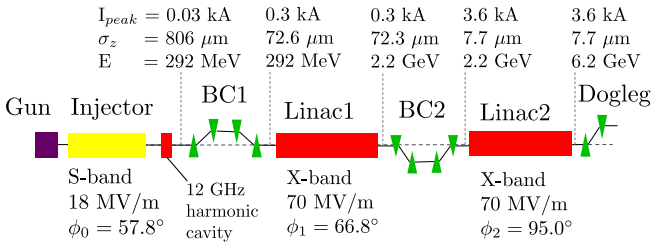

FIG. 1. Baseline design layout of an FEL linac utilizing a two-stage bunch compression scheme, based on the designs presented in [38,39].

[33]. A complete X-band FEL linac design utilizing optical linearization up to second-order can be found in [9].

Throughout the rest of this paper, a two-stage bunch compression system is considered in a predominately X-band FEL linac (see Fig. 1). However this approach could be easily applied to linacs with a single bunch compressor or linacs with more than two bunch compressors. Complete details of the accelerator can be found in Sec. VI. The two bunch compressors will be referred to as BC1 and BC2 respectively, and the layout shown in Fig. 1 will be referred to as the baseline design.

III. CAUSTICS

In a recent paper, a caustic-based approach was taken to describe current horns in strong bunch compression [28]. Small continuous perturbations in the longitudinal phase space distributions can result in intense current spikes at the head and tail of the beam when the beam passes through a dispersive region. Figure 2 illustrates this effect, showing the electron trajectories in z, s space, where z is the longitudinal position with respect to the bunch center, and s is the position along the accelerator, or in the case of Fig. 2, the position along the bunch compressor. Near the end of the compressor (which is indicated by the gray vertical line in Fig. 2), the trajectories have coalesced at the edges of the bunch, resulting in the intense current horns visible in the histogram of Fig. 2.

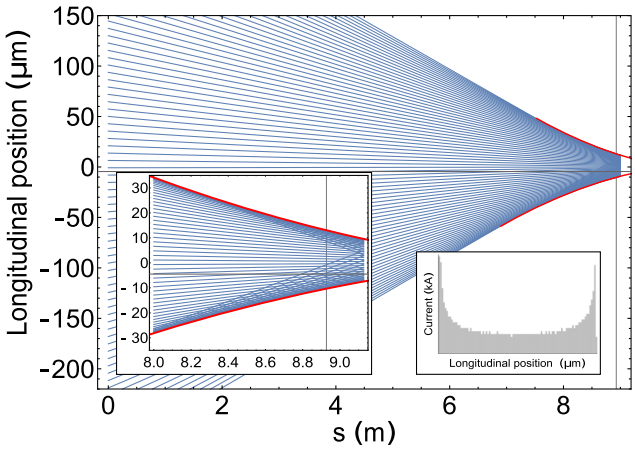

FIG. 2. Electron trajectories showing individual particles' longitudinal position, z_f, evolving with distance along a bunch compressor chicane, s. The vertical gray line at $s = 8.9$ m represents the end of the chicane. The caustic equation, Eq. (7), is shown by the bold red line. Left inset: close up of trajectories near the end of the chicane. Right inset: double-horned current profile at chicane end.

The longitudinal position of the caustics for a given set of control parameters, R_{56}, T_{566}, and U_{5666} (i.e., the first-, second-, and third order longitudinal dispersion), is (Eq. (8) in [28]),

$$\tilde{z}(z_i) = z_i - \frac{\delta(z_i)}{\delta'(z_i)} - T_{566}\delta^2(z_i) - 2U_{5666}\delta^3(z_i) \tag{7a}$$

$$\tilde{R_{56}}(z_i) = \frac{-1}{\delta'(z_i)} - 2T_{566}\delta(z_i) - 3U_{5666}\delta^2(z_i), \tag{7b}$$

where $\delta(z_i)$ is the shape of the initial longitudinal phase space or chirp, often described by a high-order polynomial and $\delta'(z_i)$ is the derivative with respect to z_i.

Equation (7) defines the envelope of the family of trajectories that form the caustic. In Fig. 2, the caustic is shown by the bold red line.

When evaluated at the end of the bunch compressor, the condition which identifies if caustics will form is [28],

$$R_{56}\delta'(z_i) + T_{566}\delta''(z_i) + U_{5666}\delta'''(z_i) + 1 = 0. \tag{8}$$

If the caustic condition [Eq. (8)] is met then the electron trajectories will form caustics resulting in the large current spikes as described by Eq. (7) and visible in Fig. 2.

IV. AVOIDING CAUSTIC-INDUCED CURRENT HORNS

Using the caustic condition described in Eq. (8) we can find a set of control variables for which the caustics *cannot* form and therefore find the conditions which prevent the current horns from developing through the dispersive region.

To determine this set of control variables we first consider a plot of the coordinates of the final and initial longitudinal positions (z_f and z_i), for each individual particle. This is shown in Fig. 3. The two turning points of Fig. 3 indicate the bifurcation points of the caustic. These coordinates correspond to the edges of the longitudinal phase space distribution, which start to curve away from a linear fit, as seen in Fig. 2.

With the aim being to find the regions where one, two, or no caustics will be present, we can use these turning points as an indication of whether we have one, two, or no bifurcation sets appearing. With this in mind we take the derivative of z_f with respect to z_i and then for ease of calculations we truncate the result including terms up to second order z_i. This gives us,

$$\frac{dz_f}{dz_i} \approx 1 + h_1 R_{56} + 2(h_2 R_{56} + h_1^2 T_{566}) z_i + 3(h_3 R_{56} + 2h_1 h_2 T_{566} + h_1^3 U_{5666}) z_i^2, \tag{9}$$

where h_1, h_2, and h_3 are the first-, second-, and third-order chip from $\delta(z_i) = h_3 z_i^3 + h_2 z_i^2 + h_1 z_i$.

Setting Eq. (9) to equal zero and rearranging for z_i identifies the caustic point(s) in z_i as,

$$z_{i,\text{bifurcation}} = \frac{h_2 R_{56} + h_1^2 T_{566}}{3(h_3 R_{56} + 2h_1 h_2 T_{566} + h_1^3 U_{5666})} + \frac{\sqrt{(h_2 R_{56} + h_1^2 T_{566})^2 - 3(1 + h_1 R_{56})(h_3 R_{56} + 2h_1 h_2 T_{566} + h_1^3 U_{5666})}}{3(h_3 R_{56} + 2h_1 h_2 T_{566} + h_1^3 U_{5666})}. \tag{10}$$

The points where $z_{i,\text{bifurcation}}$ [Eq. (10)] reaches the maximum or minimum longitudinal position of the initial distribution (denoted by $z_{\min/\max}$), indicates a boundary, bordering regions of one and two caustics forming, or zero and one caustic forming. That is, when $z_{i,\text{bifurcation}}$ of Eq. (10), equals the maximum or minimum of the range of possible z_i values, this indicates the border between when two turning points are visible in Fig. 3 and when there is one. This corresponds to two caustic-induced current horns or one. Therefore, the border between the caustic regions is defined by the set of variables, (R_{56}, T_{566}, U_{5666}, h_1, h_2, h_3), evaluated for a given initial bunch with $z_{\min/\max}$, such that $f(R_{56}, T_{566}, U_{5666}, h_1, h_2, h_3; z_{\min/\max}) = 0$, with,

$$\begin{aligned} &f(R_{56}, T_{566}, U_{5666}, h_1, h_2, h_3; z_{\min/\max}) \\ &\quad = 1 + h_1 R_{56} + 2h_2 R_{56} z_{\min/\max} \\ &\qquad + 3h_3 R_{56} z_{\min/\max}^2 + 2T_{566} h_1^2 z_{\min/\max} \\ &\qquad + 6T_{566} h_1 h_2 z_{\min/\max}^2 + 3h_1^3 U_{5666} z_{\min/\max}^2. \end{aligned} \tag{11}$$

Using Eq. (11) we can inspect how the caustics will form in T_{566}, U_{5666} space by holding constant h_1, h_2, and h_3 (which are defined by the incoming bunch) and by choosing a value for R_{56} which is determined by the compression ratio requirements. This allows us to take a slice through the 6-dimensional parameter space defined above by the set of variables (R_{56}, T_{566}, U_{5666}, h_1, h_2, h_3),

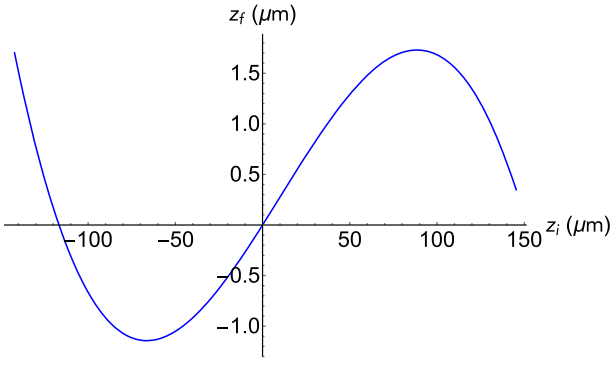

FIG. 3. Correlation between the final longitudinal position of a particle leaving a bunch compressor for a given initial longitudinal position for a particle entering a bunch compressor.

leaving us with an analytic expression for the caustic region borders,

$$\begin{aligned} T_{566} = -\frac{1}{2h_1 z_{\min/\max}(h_1 + 3h_2 z_{\min/\max})}[&1 + h_1 R_{56} \\ &+ 2h_2 R_{56} z_{\min/\max} \\ &+ (3h_3 R_{56} + 3h_1^3 U_{5666}) z_{\min/\max}^2] \end{aligned} \tag{12}$$

where $z_{\min/\max}$ is the maximum or minimum of the initial longitudinal distribution.

Figure 4 shows these boundaries between the regions of zero, one or two caustics, as described by Eq. (12). In this example the value of R_{56} was -11.8 mm and the values of the longitudinal chirp used are,

$$\begin{aligned} h_1 &= 81.0563\ \text{m}^{-1} \\ h_2 &= 5929.08\ \text{m}^{-2} \\ h_3 &= 1.30211 \times 10^7\ \text{m}^{-3}, \end{aligned}$$

where the longitudinal chirp is described by a third-order polynomial, $\delta = h_3 z_i^3 + h_2 z_i^2 + h_1 z_i$.

Also in Fig. 4 are histograms of the electron density (at the end of the dispersive region) for various combinations of T_{566} and U_{5666}, showing regions of one, two, or zero caustic current horns forming. These correspond to single fold caustics appearing at the head or tail of the beam, two fold caustics forming a cusp catastrophe, or no caustic formation resulting in a relatively flat current profile. Figure 4 shows that for an FEL linac there should exist a region in T_{566}, U_{5666} parameter space where caustics (and the associated current horns) will not form.

Using a similar approach to deriving Eq. (12), we can use Eq. (11) to find the caustic regions in h_2, h_3 space, for a given first-order chirp, h_1. Then the boundaries are,

$$\begin{aligned} h_2 = &-\frac{1 + h_1 R_{56} + 2h_1^2 T_{566} z_{\min/\max}}{2z_{\min/\max}(R_{56} + 3h_1 T_{566} z_{\min/\max})} \\ &+ \frac{3(h_3 R_{56} + h_1^3 U_{5666}) z_{\min/\max}^2}{2z_{\min/\max}(R_{56} + 3h_1 T_{566} z_{\min/\max})}. \end{aligned} \tag{13}$$

Equation (13) is shown in Fig. 5 for the second bunch compressor (BC2) in a two-stage compression scheme,

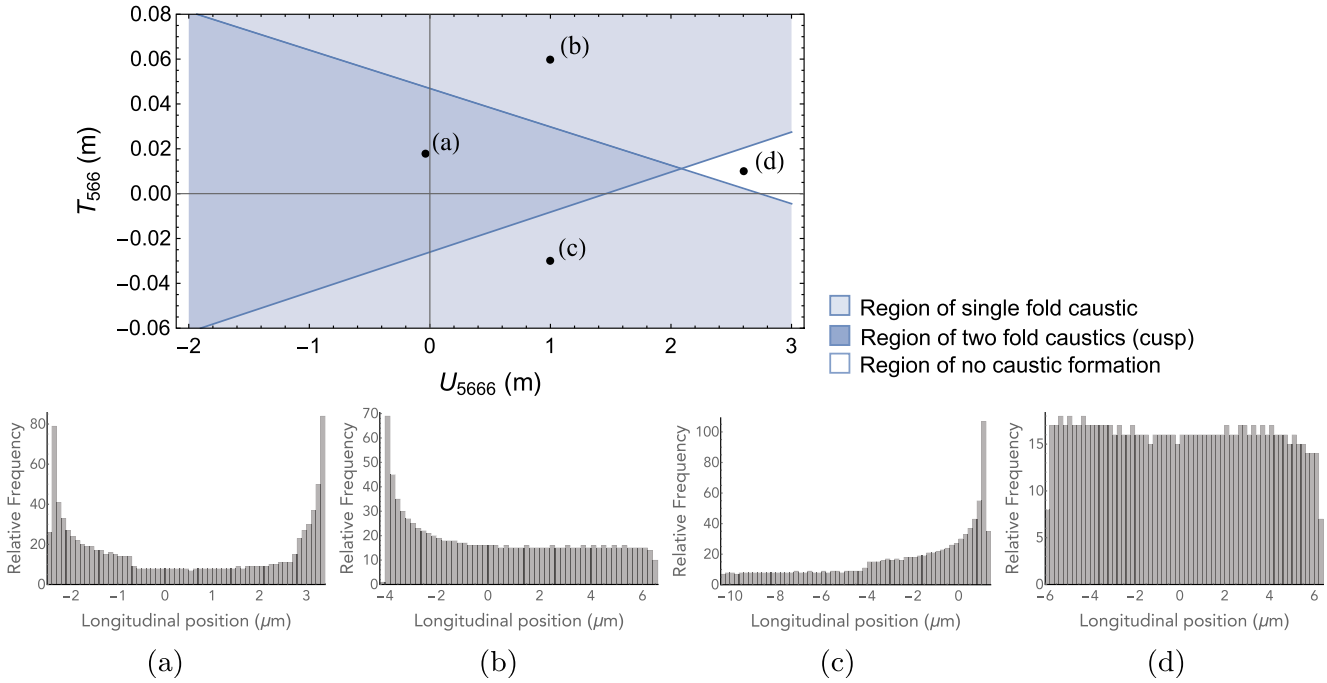

FIG. 4. Boundaries between regions of one and two caustic current horns, and zero and one caustic current horn. The analytical expression for these boundaries is Eq. (12). Here they are shown for an arbitrary R_{56} value of -11.8 mm, and first-, second-, and third-order longitudinal chirp values of $h_1 = 81.0563$ m^{-1}, $h_2 = 5929.08$ m^{-2}, and $h_3 = 1.30211 \times 10^7$ m^{-3} respectively. [Chirp values h_1, h_2, and h_3 are defined in Eq. (1).]

where BC2 is a standard 4-dipole chicane where $T_{566} = -3/2R_{56}$ and $U_{5666} = 2R_{56}$, where R_{56} is -11.8 mm. Included in Fig. 5 is a marker labeled (1) which indicates the coordinates of the distribution mentioned earlier ($h_1 = 81.06$ m^{-1}, $h_2 = 5929.08$ m^{-2}, and $h_3 = 1.30211 \times 10^8$ m^{-3}), revealing how these typical operating conditions position the working point in the region that will lead to caustic-induced current horns.

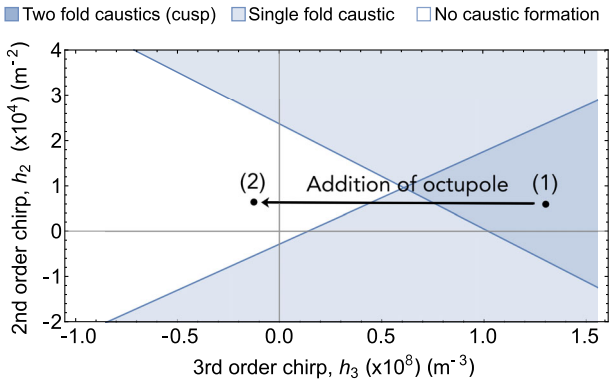

FIG. 5. Regions of h_2, h_3 space where single, multiple, or zero caustics are expected to be found. Position (1) indicates the working point of a standard chicane with $R_{56} = -11.8$ mm, and with the same initial distribution parameters used in Fig. 4. Through addition of an octupole to BC1, the working point can be moved from position (1) to position (2) which lies in a noncaustic region.

V. BUNCH COMPRESSORS DESIGNED TO AVOID CAUSTICS

In the previous section we found that there should exist regions in parameter space where caustics (and the associated current horns) will not form. Figure 4 [from Eq. (12)] and Fig. 5 [from Eq. (13)] present two ways to suppress the current horns. The first approach shows that caustics can be avoided by varying T_{566} and/or U_{5666} of BC2. The second approach shows that caustics can be avoided by varying the second- and/or third-order chirp (h_2 and/or h_3) of the bunch that arrives at BC2. The first approach can be achieved through using octupoles to vary U_{5666}, similarly to how sextupoles can be used to vary the 2nd order longitudinal dispersion [33]. The second approach can be achieved through adding an octupole to the center of the first bunch compressor (BC1), well upstream of BC2, to vary the higher-order chirp of the bunch arriving at BC2. Leaving BC1, the bunch encounters the longitudinal wakefields, which impart a cubic chirp onto the beam [12]. Therefore the octupole added to BC1 must overcorrect for the effect the longitudinal wakefields will have on the third-order chirp, in order to position the bunch parameters in an optimal position in h_2, h_3 space for avoiding caustics (see Fig. 5).

Figure 4 indicates that we would require a T_{566} of approximately 15 mm and a U_{5666} value of greater than 2 m. For the standard 4-dipole chicane considered here, for which R_{56} is -11.8 mm, the value of T_{566} is already close to

what is required at 17.7 mm (where $T_{566} = -3/2R_{56}$). Therefore octupoles could be used to alter U_{5666}, whilst keeping T_{566} fairly constant. It should be noted that if a particular arrangement of initial distribution and longitudinal dispersion values required the value of both T_{566} and U_{5666} to be varied substantially away from their original position, then both sextupoles and octupoles could be implemented to achieve the required T_{566} and U_{5666} values. Such a scenario may present itself if harmonic linearization is not used to linearize the second-order chirp, or if a dog-leg or nonstandard chicane is used. Essentially, sextupoles can be used to vary T_{566} to move the working point position vertically in Fig. 4, and octupoles can be used to vary U_{5666} to move the working point position horizontally in Fig. 4.

In order to achieve the value of U_{5666} for BC2 required (>2 m), strong octupole magnets would be required, introducing strong chromatic aberrations. So instead, an octupole was added to the center of BC1, where weaker field strengths are needed. The purpose behind this approach is a little different. Here we use an octupole magnet in BC1 to alter the third-order chirp of the bunch that arrives at BC2, rather than directly altering the dispersion values of BC2. Leaving BC1, the bunch encounters the longitundal wakefields of Linac1, which impart a cubic chirp onto the beam [12]. Therefore the octupole added to BC1 is used to overcorrect for the effect the longitudinal wakefields will have on the 3rd order chirp, in order to position the bunch parameters in an optimal position in h_2, h_3 space for avoiding caustics. This position in h_2, h_3 space is marked as (2) in Fig. 5.

Several different configurations of BC1 and BC2 were considered, all of which capable of achieving a wide range of T_{566} and U_{5666} values for a given R_{56} (i.e., for a given compression ratio). Figure 6 shows the layouts of two

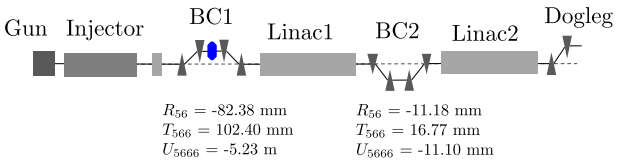

(a) Layout 1: linac design including the addition of an octupole magnet to BC1 to avoid current horn formation.

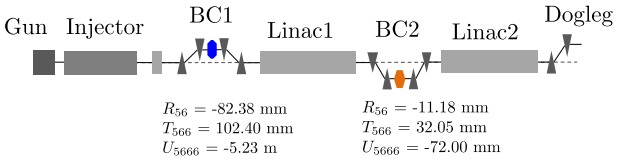

(b) Layout 2: linac design including an octupole magnet in BC1, and a sextupole in BC2 for further CSR optimization.

FIG. 6. Layouts of the FEL linac using an S-band injector and X-band linac. Section VI compares simulation results of these two configurations with the baseline design shown in Fig. 1.

X-band FEL linacs with additional optical elements included to allow for the manipulation of the longitudinal phase space. Figure 6(a) shows what will be referred to as Layout 1, which includes the octupole magnet in BC1. In Sec. VI A this design will be compared with the baseline design of Fig. 1, as well as to a third design, Layout 2 (Fig. 6(b)) which will be described in Sec. V B.

ELEGANT simulation of the layout shown in Fig. 6(a) (i.e., with an octupole added to BC1) finds that the longitudinal distribution parameters of the bunch arriving at the BC2 entrance has the following fitted parameters;

$$h_1 = 81.7245 \text{ m}^{-1}$$
$$h_2 = 6408.13 \text{ m}^{-2}$$
$$h_3 = -1.2575 \times 10^7 \text{ m}^{-3}$$

where the longitudinal chirp is described by a third-order polynomial $\delta = h_3 z_i^3 + h_2 z_i^2 + h_1 z_i$.

The new values of the h_2, and h_3 of the bunch arriving at BC2 (having been altered by the octupole in BC1), move the working point in Fig. 5 to the region of no caustic formation. In Sec. VI we will verify this analytical approach with ELEGANT simulations.

A. Optics through BC1

The values of the longitudinal dispersion for the new BC1 design are $R_{56} = -82.36$ mm, $T_{566} = 124.57$ mm, and $U_{5666} = -2.83$ m. The R_{56} was achieved through a bending angle of 5.25° and a drift length of 4.544 m between dipole 1 and dipole 2, and between dipole 3 and dipole 4. Figure 7 shows the first order optics through the chicane. The octupole magnet is located at the center of the chicane where the horizontal dispersion is greatest, and has a length of 0.3 m and normalized field strength of $K_3 = 1173.12$ m^{-3}.

At the end of the chicane, the second order horizontal and angular dispersion, T_{166} and T_{266} return to zero. This ensures that the dispersion-induced emittance growth associated with the large energy spread is kept to a minimum [40].

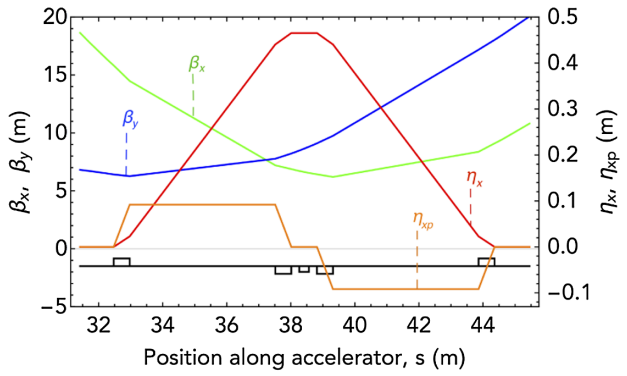

FIG. 7. Optics through BC1, showing β_x (green), β_y (blue), η_x (red), and η_{xp} (orange).

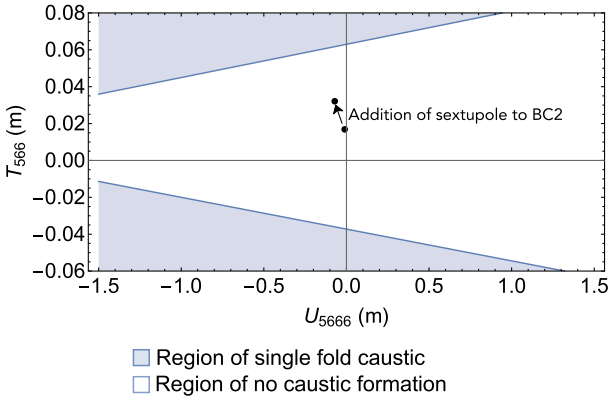

FIG. 8. Regions indicated where caustics are expected to be found and where they are absent. The boundaries between these regions are given by Eq. (12). The addition of a weak sextupole to BC2 changes the T_{566}, U_{5666} coordinate of the working point, moving it closer to the upper boundary, and consequently shifting some of the current from the tail to the head of the bunch.

B. Further optimization: Addition of a sextupole magnet to BC2

Further improvement can be made through positioning the working point in T_{566}, U_{5666} space closer to the upper caustic boundaries of Fig. 4, whilst remaining within the caustic free region. This is because whilst the current horn formation has been mostly suppressed, a remnant peak can still be seen at the BC2 exit [this will be seen Fig. 11(b)]. Moving the working point closer to the upper caustic boundary (see Fig. 8) shifts the bunch charge away from the tail of the bunch and closer to the head. Ensuring the tail has a lower current than the head, further aids emittance preservation as the CSR that leads to CSR-induced emittance growth is predominately produced by the tail of the bunch. This translation in T_{566}, U_{5666} space can be achieved through adding a weak sextupole to the center of BC2.

C. Optics through BC2

The values of the longitudinal dispersion for the new design of BC2, with the inclusion of a weak sextupole magnet, are $R_{56} = -11.18$ mm, $T_{566} = 32.10$ mm and $U_{5666} = -72.19$ mm. The R_{56} was achieved through a dipole bending angle of 1.35° and a drift length of 9.667 m between dipole 1 and dipole 2, and between dipole 3 and dipole 4. Figure 9 shows the first order optics through the chicane. The sextupole has a length of 0.2 m and normalized field strength of $K_2 = 11.03$ m^{-2} and is located at the center of the chicane.

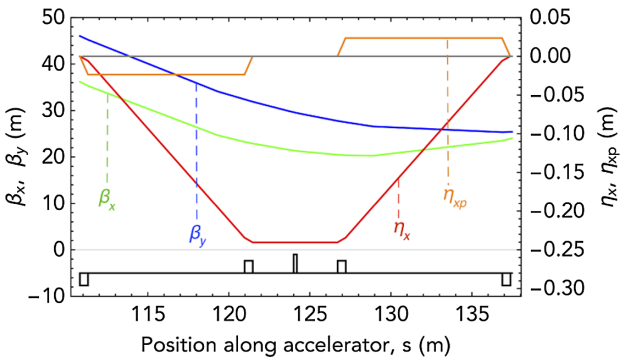

FIG. 9. Optics through BC2, showing β_x (green), β_y (blue), η_x (red), and η_{xp} (orange).

D. Other CSR suppression techniques

In addition to the suppression of CSR by eliminating current horns by suitable configuration of additional optical elements (which is the main result of this paper), a few techniques have been employed. These techniques are consistent across all scenarios presented in Sec. VI, meaning that the improvement in emittance preservation due to the removal of the current horns alone can be seen in Sec. VI.

The CSR wakefield potential changes the particle energy along the longitudinal direction, and also affects the transverse motion through the dispersive region [20,41,42]. This transverse kick can be partially canceled through ensuring that BC1 and BC2 bend the beam in opposite directions [5,21,43], i.e., the bending angle of dipole 1 of BC1 has the opposite sign of dipole 1 of BC2.

In addition, the beta functions were minimized toward the end of BC2 where the bunch length is shortest and the effect of CSR strongest. This is a commonly employed technique described in [44,45].

VI. PARTICLE TRACKING SIMULATIONS

In this section we present the results of 6D ELEGANT [18,46] simulations of the three linacs: a. Baseline design with no additional multipoles (see Fig. 1); b. Layout 1 which includes an octupole added to the center of BC1 [see Fig. 6(a)]; c. Layout 2 which includes the same octupole added to BC1 as well as a sextupole added to BC2 [see Fig. 6(b)].

The beam distribution input for the ELEGANT simulations was modeled on an S-band injector producing a beam with an initial energy of 131.2 MeV, an RMS bunch length of 807 μm, and a normalized transverse emittance of 0.2729 mm mrad with a total bunch charge of 250 pC. Important parameters of peak current (I_{peak}), RMS bunch length (σ_z), and beam energy (E) are shown in Fig. 1 at various locations along the linac. The residual correlated energy spread is removed in the final 85 m of linac2, mainly through longitudinal wakefields.

Consistent in all three layouts (Baseline of Fig. 1 and, Layout 1 and Layout 2 of Fig. 6) is an S-band injector followed by an X-band harmonic cavity to linearize the 2nd order longitudinal phase space [8]. Also consistent to all three layouts is a laser heater, used to increase the uncorrelated energy spread to provide strong Landau damping to

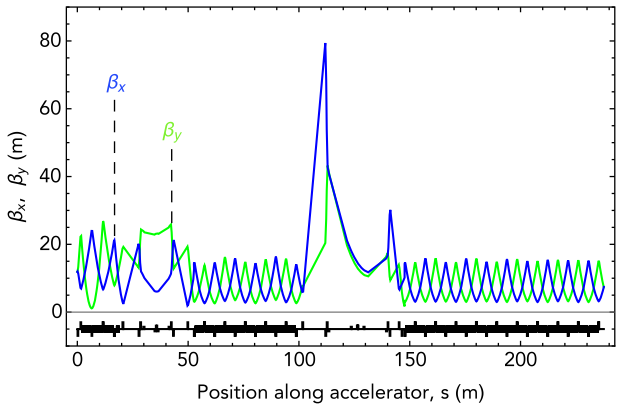

FIG. 10. Beta functions along the linac, with β_x (blue) and β_y (green).

suppress microbunching instability [47]. Specific details of the bunch compressors can be found in Sec. V. Figure 10 shows the beta functions along the entire linac.

Figure 11 shows the longitudinal phase space distributions and current profiles for each of the 3 layouts, demonstrating that the octupole magnet is capable of reducing the current horns. A small remnant peak at the tail of the bunch can still be seen in Fig. 11(b). This small peak is due to the approximation used in describing the longitudinal phase space as a cubic distribution. This small peak at the tail of the bunch sparked the investigation of adding a sextupole to BC2 in an attempt to shift some of the current from the tail to the head of the bunch. This creates a small but noticeable improvement to the current profile with the benefit of reduced CSR reflected in the projected emittances listed in Table I. However, the majority of the improvement to projected emittance is established by the inclusion of just one octupole magnet.

Table I lists the emittances (projected and slice) for the three linac configurations, showing that it is possible to reduce the projected emittance by 30.1% with an octupole included in BC1. The addition of a weak sextupole to BC2 [Fig. 6(b)], reduces the projected emittance by 38.8%. For this layout, the reduction in the CSR-induced emittance growth is 48.9%. Further, the rms energy spread is also improved by 20.7%, which allows for more uniform lasing along the bunch.

Figure 12 shows the longitudinal phase space distributions and current profiles with the laser heater turned off, and CSR not included in the simulations for each of the 3 layouts. These plots show the caustic current horns more pronounced. CSR and to a lesser extent, the energy mixing introduced by the laser heater, have the effect of smearing out the caustics. In the simulations that produced Fig. 12(b) and Fig. 12(c), the octupole magnetic field strength, K_3, was 2000 m^{-3}, reoptimized to account for the change in particle energy induced by CSR. The sextupole field strength relevant to Fig. 12(c) remained unchanged at $K_2 = 11.03$ m^{-2}. Similarly to Figs. 11(b) and 12(b) shows a small peak visible at the head of the bunch, due to the inherent asymmetry of the compression process where the particles at the tail of the bunch (with negative values of z_i)

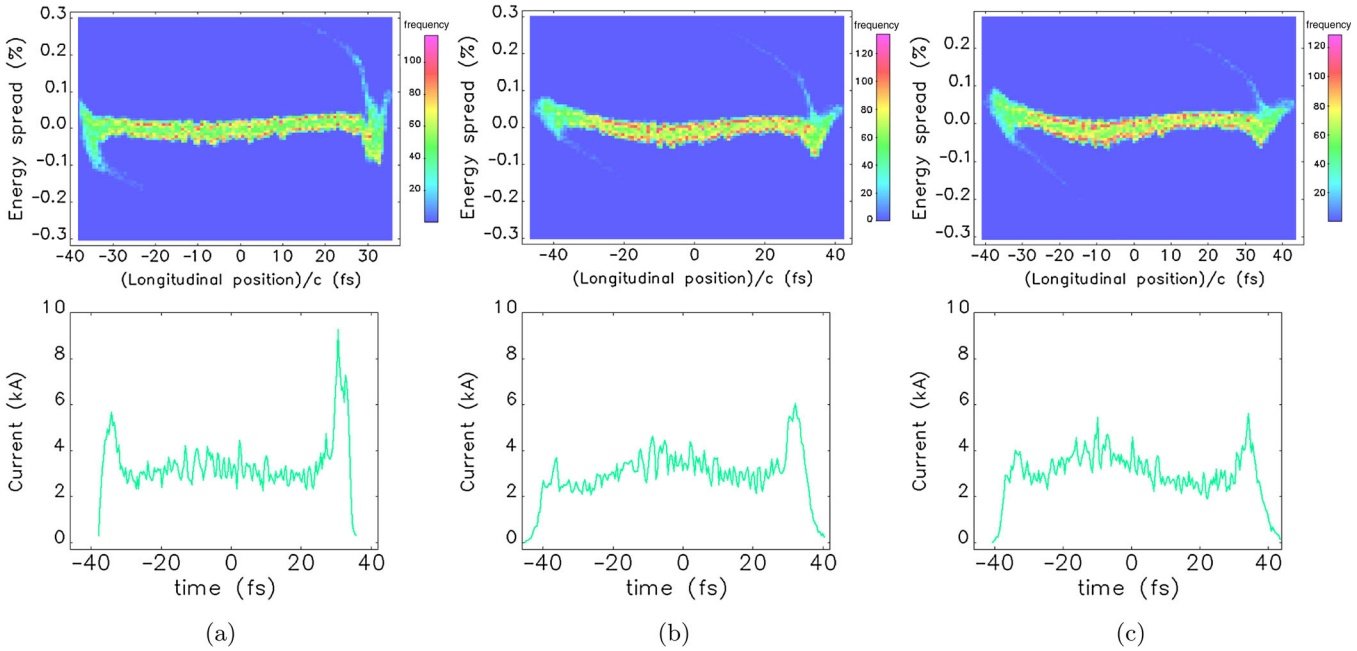

FIG. 11. Longitudinal phase space distribution and current profiles at the end of the linac for the three layouts described in Figs. 1, 6(a), and 6(b). (a) baseline layout which does not include any multipoles. (b) Layout 1 which includes an octupole magnet in BC1. (c) Layout 2 which includes the same octupole in BC1 as well as a weak sextupole magnet in BC2. Note the head of the bunch corresponds to negative values of longitudinal position.

TABLE I. Beam properties at the end of the final linac section, for (a) Baseline layout, (b) Layout 1: which includes BC1 octupole magnet [Fig. 6(a)], (c) Layout 2 which includes BC2 sextupole magnet [Fig. 6(b)].

Parameter	Symbol	Units	Baseline	Layout 1	Layout 2
Bunch length	σ_z	μm	6.65	6.75	6.68
Horizontal bunch size	σ_x	μm	0.376	0.306	0.267
Vertical bunch size	σ_y	μm	0.161	0.162	0.163
Energy spread	$\sigma_{\Delta E/E}$	%	0.0371 (core)	0.0292	0.0281
Peak current	I_{peak}	kA	3.02 (core)	3.02	3.09
Total compression ratio	CR	⋯	121.38[a]	119.6	120.8
Bunch charge	Q	pC	250	250	250
Electron energy	E	GeV	6.16	6.16	6.16
Projected horizontal emittance	$\epsilon_{n,x}$	mm mrad	1.394	0.974	0.842
Mean horizontal slice emittance	$\epsilon_{s,n,x}$	mm mrad	0.386	0.392	0.377
Projected vertical emittance	$\epsilon_{n,y}$	mm mrad	0.274	0.273	0.274
Mean vertical slice emittance	$\epsilon_{s,n,y}$	mm mrad	0.255	0.249	0.246

[a]Note the bending angles of BC2 were reduced by less than 0.01% to bring the compression ratio down to be in-line with Layout 1 and Layout 2.

will be compressed to a greater degree than particles at the head [this is evident from Eq. (5)].

A. Discussion on emittances

Table I shows that it is possible to reduce the projected emittance by 30.1% with an octupole included in BC1, and the addition of a weak sextupole to BC2 [Fig. 6(b)], reduces the projected emittance by 38.8%.

The cost of adding octupole magnets to a chicane is the introduction of geometric aberrations. This is reflected in the slight increase in the mean slice emittance shown in Table I. However this small increase in slice emittance is recovered through the addition of a sextupole, and nevertheless is not large enough to have a significant influence on the gain length and power output of the undulator section.

Figure 13 shows the correlation between the octupole field strength K_3, and reduction in projected emittance growth. As the field strength of octupole is increased, U_{5666} also increases, and the working point on Fig. 4 moves from the region of two current horns forming, to no current horns forming. Through this progression, the current horns

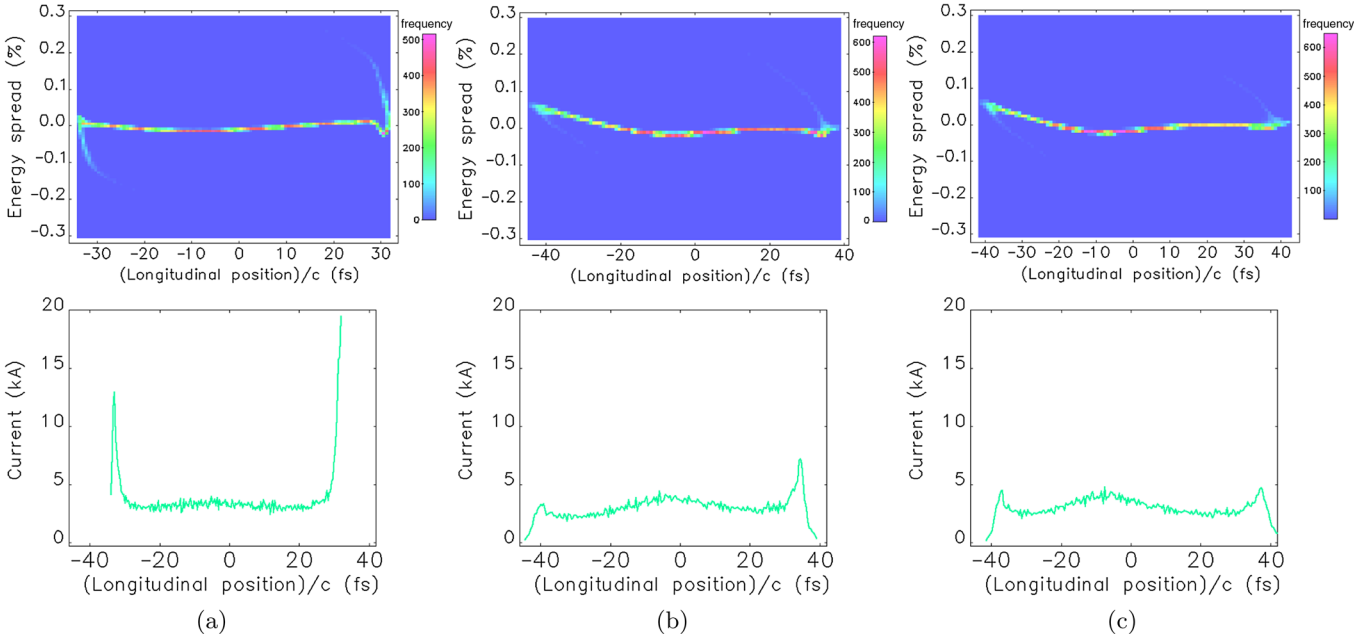

FIG. 12. Longitudinal phase space distribution and current profiles at the end of the linac for the three layouts described in Figs. 1, 6(a), and 6(b), without CSR or laser heating included in the simulation. (a) baseline layout which does not include any multipoles. (b) Layout 1 which includes an octupole magnet in BC1. (c) Layout 2 which includes the same octupole in BC1 as well as a weak sextupole magnet in BC2. Note the head of the bunch corresponds to negative values of longitudinal position.

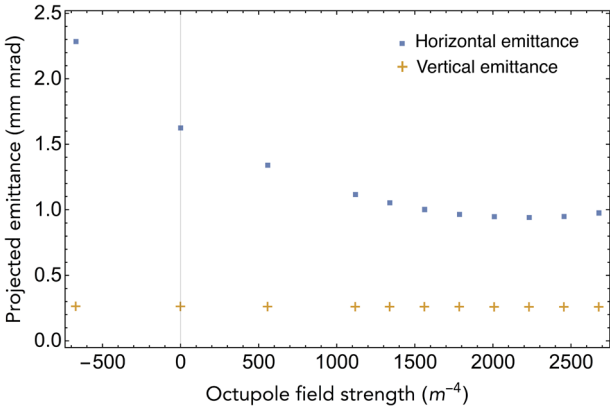

FIG. 13. Projected horizontal (blue square) and vertical (orange +) emittances produced with the Layout 2 design [Fig. 6(b)] with various octupole field strengths.

become smaller to the point of almost disappearing. With reduced current at the head and tail of the bunch, the CSR-induced emittance growth is quelled. This is evident in the horizontal emittance in Fig. 13. The vertical emittance is preserved at 0.274 mm mrad, and remains unchanged with octupole field strength.

Interestingly, the horizontal emittance decreases to a minimum and then at large values of K_3 it gradually starts to rise again (Fig. 13). This is likely due to the competing effects of improved emittance from CSR suppression and emittance growth from chromatic aberrations.

The longitudinally sliced properties of the bunch at the end of the linac can be seen in Fig. 14. Figures 14(a) and 14(b) show that there is only a small difference in the slice emittances for the three FEL layouts. This is in agreement with much of the literature which states that CSR is likely to lead to projected emittance growth whilst leaving the slice emittance relatively unchanged [21,27]. The core of the bunch sees only a small increase in horizontal emittance of 8% whilst the bunch head and tail horizontal emittance grow to a greater degree by, at the largest, a factor of 1.9. This increase in slice emittance at the edges of the bunch is consistent across all three designs, however the effect on FEL performance would be less significant in Layout 1 and 2, where the current horns are reduced leaving less charge in the regions of larger slice emittance.

Figures 14(c) and 14(d) show the centroid offset and mean value of x' for each slice, revealing that Layout 1 and to an even greater extent Layout 2, reduce the variation in these two parameters along the length of the bunch. In other words, this confirms that the inclusion of an octupole (which can be even further improved by the inclusion of a sextupole magnet) to the bunch compressors, through preventing the current horns from forming, reduced the effect of CSR, evidenced by the reduced centroid offsets along the bunch and associated reduced projected transverse emittance.

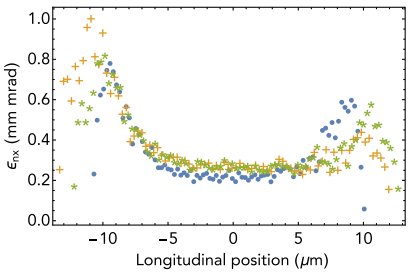

(a) Slice horizontal emittance

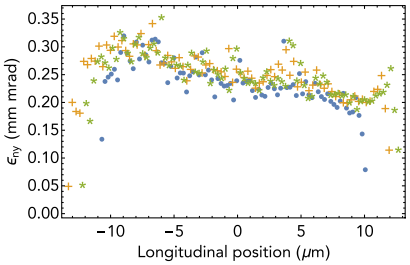

(b) Slice vertical emittance

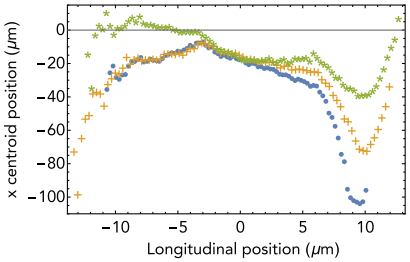

(c) Horizontal offset of slices

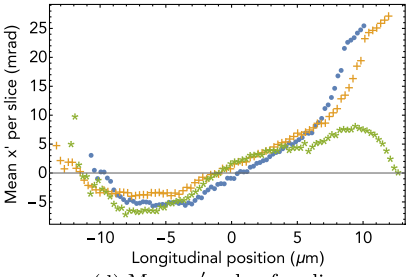

(d) Mean x' value for slices

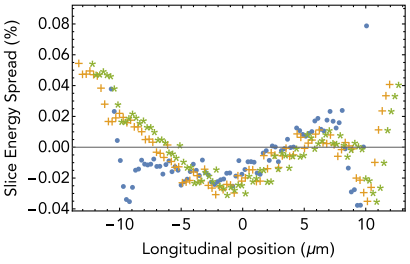

(e) Slice energy spread

FIG. 14. Slice properties of the bunch at the end of the linac for the X-band Baseline design (blue circle), Layout 1 (orange +), and Layout 2 (green asterisk). The x centroid offset and the variation in x' along the length of the bunch cause increased projected emittance growth of the baseline design.

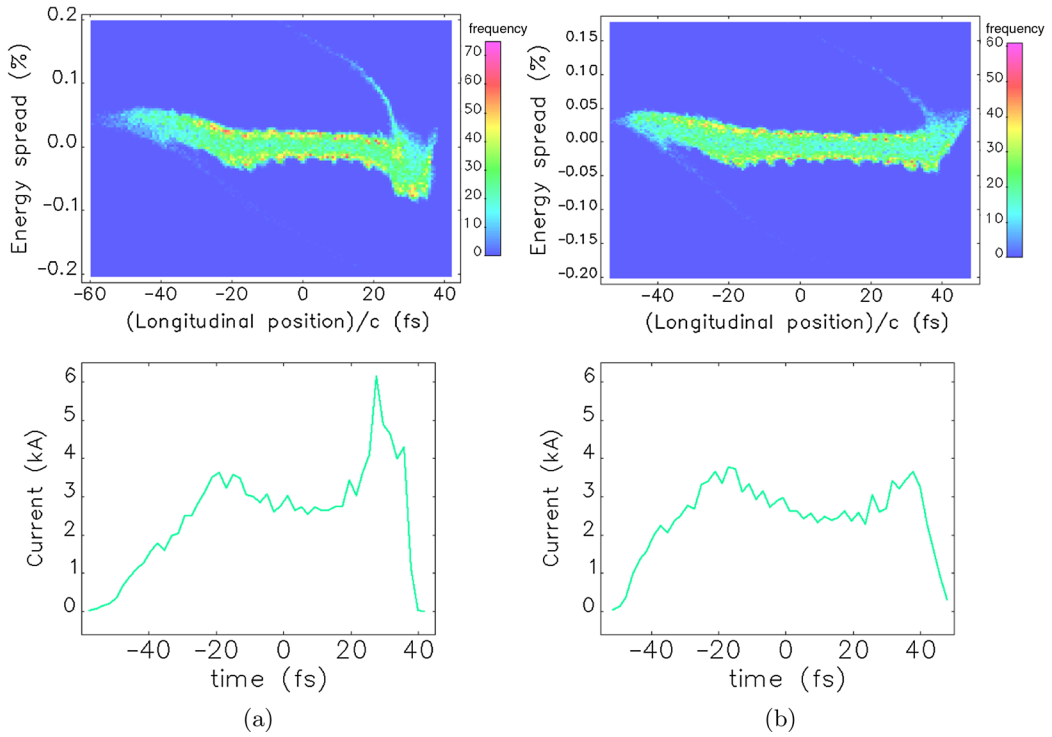

FIG. 15. Longitudinal phase space distribution and current profiles at the end of the S-band linac with CSR and laser heating included for (a) without any octupole magnets and (b) with an octupole included in BC2. Note the head of the bunch corresponds to negative values of longitudinal position.

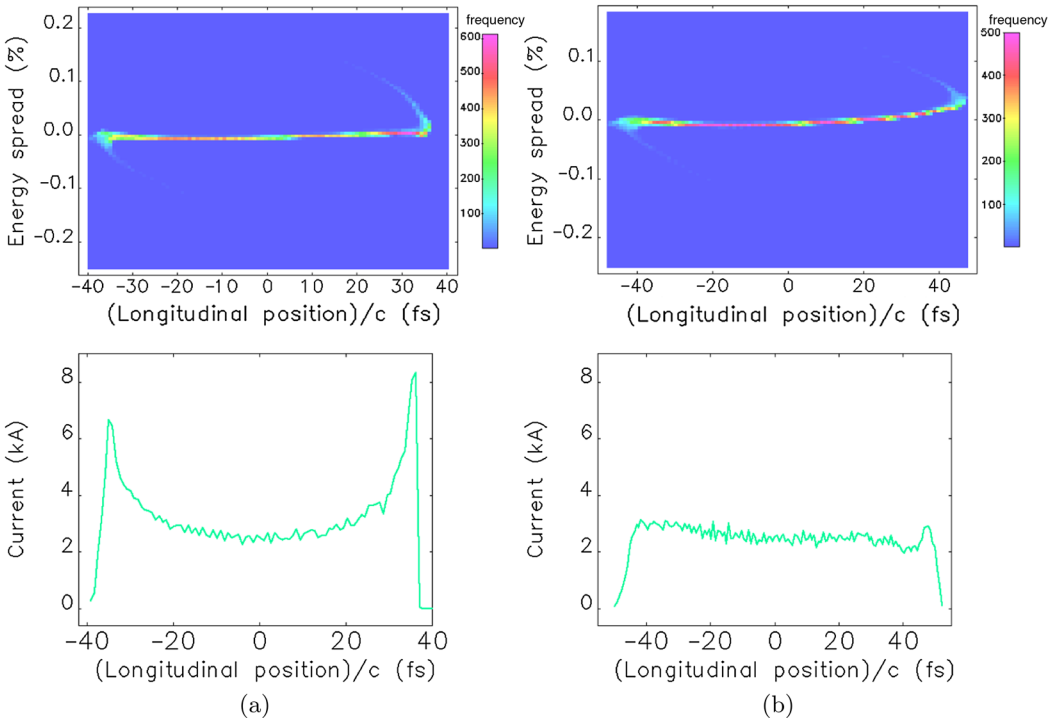

FIG. 16. Longitudinal phase space distribution and current profiles at the end of the S-band linac without CSR or laser heating included in the simulation for (a) without any multipole magnets and (b) with an octupole included in BC2. Note the head of the bunch corresponds to negative values of longitudinal position.

B. S-band linac comparison

X-band linacs typically pose a more difficult scenario than S-band linacs due to the stronger wakefields and because for a given bunch length, the bunch will see a greater portion of the rf curve when the rf frequency is in the X-band compared to S-band. This second point will mean that a greater degree of curvature is impressed onto the bunch. In this section we follow the same method presented earlier but instead shown on an S-band linac.

The results of the current horn suppression in an S-band linac are shown in Figs. 15 and 16, for with CSR and laser heating and without, respectively. The S-band linac consisted of two bunch compressor chicanes (however again, it should be noted that this method is applicable to any combination of bunch compressors).

With the absence of any higher-order magnets in the chicanes, the current spikes are clearly visible in Fig. 16(a). After the inclusion of an octupole (this time in the second bunch compressor) of normalized field strength $K_3 = -1007\ \mathrm{m}^{-3}$, the current spikes have been diminished [see Fig. 16(b)]. Figure 17 shows the slice properties (slice emittances, mean x' position, slice energy spread and x centroid position) for this S-band example before and after the inclusion of an octupole. Similarly to the X-band case, the slice emittance in x and y is maintained between the scenarios of with and without an octupole. The main difference is the x-centroid position is more consistent along the bunch after the inclusion of the octupole. This is true of both the X-band and S-band cases [see Figs. 14(d) and 17(d)].

Whilst in the case of the X-band linac, the energy spread in the core of the bunch was slightly worse with the octupole and sextupole magnet [see Fig. 14(e)], the same cannot be said for the S-band case. For the S-band case, the energy spread along the bunch at the end of the linac with the octupole performs just as well (or marginally better) when compared to without the octupole [see Figs. 17(e) and 15]. When CSR and laser heating are not included, the slight curvature in the energy spread along the bunch introduced by the octupole is more visible (see Fig. 16).

VII. DISCUSSION

Consider any (T_{566}, U_{5666}) coordinates in Fig. 4. As this coordinate is moved vertically (in the direction of increasing T_{566}), the current is redistributed more toward the head of the bunch. This statement is true regardless of which of the four regions the working position coordinates is in. For example, if the (T_{566}, U_{5666}) coordinates were initially in the region where two caustics form (i.e. where two current peaks are seen), moving closer toward the upper boundary will cause the bunch head peak to be larger and the bunch tail peak to be reduced. In both Figs. 11(b) and 12(b) (which show the current profiles generated with CSR and

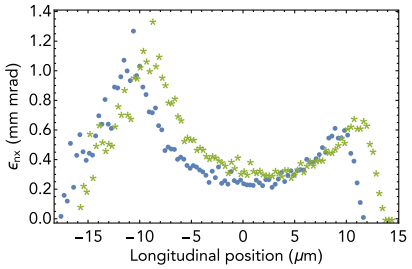

(a) Slice horizontal emittance

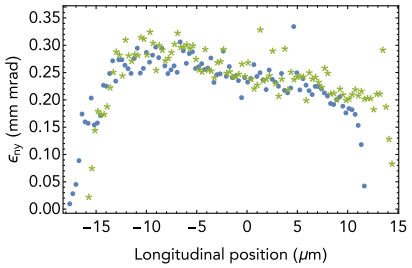

(b) Slice vertical emittance

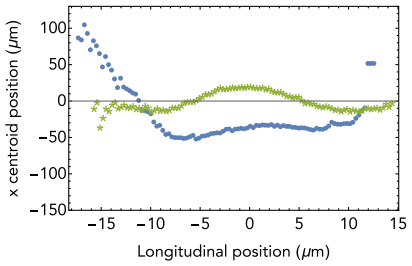

(c) Horizontal offset of slices

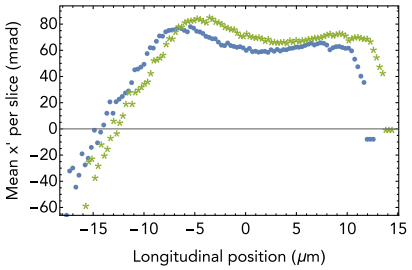

(d) Mean x' value for slices

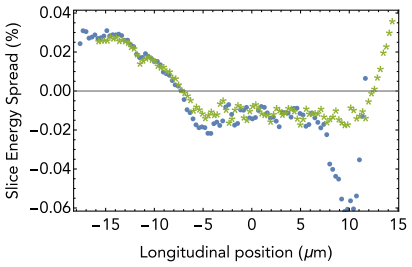

(e) Slice energy spread

FIG. 17. Slice properties of the bunch at the end of the S-band linac for without an octupole (blue circle), and with an octupole (green asterisk). The x centroid offset and the variation in x' along the length of the bunch cause increased projected emittance growth of the baseline design.

laser heating, and without, respectively), the small peak at the head of the bunch can be diminished with the aid of a weak sextupole magnet in BC2. This is because including the sextupole magnet moves the working point coordinates in Fig. 4 closer to the upper boundary, shifting the relative heights of the head and tails current peaks in favor of the head of the bunch.

The current profiles of Fig. 11(c), Fig. 12(c) both show some small undulating structure, and not a perfectly flat current profile. This can be explained by the current density modulation expected in the vicinity of the caustics. In a recent paper [28], the caustics present in strong bunch compression were identified as a Butterfly Catastrophe [48,49], and it was shown how the density of trajectories at the core of the bunch can be nonuniform when still in the vicinity of the caustics.

An alternative approach to this problem of current spike suppression, could be to find the set of parameters which eliminates both the second and third order coefficients of z_i in Eq. (6). Whilst this is a valid approach, the caustic-based approach presented in this paper, is a more general approach and conveys additional information that is not discernable if one were to approach the problem purely as a third-order chirp problem in the way described in the previous sentence. Whilst treating the problem through eliminating the coefficients of the second and third order terms on Eq. (6), would find a caustic free solution, it also obscures other possible solutions in regions where caustics (and the associated current horns) would be avoided. In Fig. 5, it can be seen that a large range of values in h_2 and h_3 space are candidates for producing a current profile absent of spikes. This allows for exploration of the margins of error permissible in beam and magnet parameters, as well as opening the possibility for redistribution of current as the working point is moved within the caustic-free region of Fig. 5. Further information on this second point can be found in Ref. [28]. In addition, the technique presented in this paper can be expanded to include higher-order terms if required. In the cases presented in this paper, including terms up to third order appears to be sufficient for the purpose of suppressing the current horns.

Finally the small peaks still visible in Figs. 11(c) and 12(c) can be suppressed completely through increasing the strength of the octupole magnet. However increasing the octupole field strength further also increases the geometric and chromatic aberrations. This concept is also illustrated in Fig. 13. It can be assumed that if the chromatic and geometric aberrations could be more adequately addressed (or balanced) then the current spikes could be further reduced.

VIII. CONCLUSION

In this paper we have demonstrated through both analytical calculations and numerical simulations, a technique to avoid current horns from forming in strong bunch compression that is typical of FEL linacs. This was achieved through consideration of the underlying caustic formation in electron trajectories and employing a suitable configuration of additional optical elements located within the bunch compressors. The result is suppressed current horns, significantly reduced CSR-induced projected emittance growth and reduced energy spread along the bunch.

ACKNOWLEDGMENTS

This research was undertaken in collaboration with the Accelerator Science group at the Australian Synchrotron, Victoria, Australia.

[1] P. Emma *et al.*, First lasing and operation of an ångstrom-wavelength free-electron laser, Nat. Photonics **4**, 641 (2010).

[2] H. Tanaka, M. Yabashi *et al.*, A compact X-ray free-electron laser emitting in the sub-ångström region, Nat. Photonics **6**, 540 (2012).

[3] W. Ackermann *et al.*, Operation of a free-electron laser from the extreme ultraviolet to the water window, Nat. Photonics **1**, 336 (2007).

[4] E. Allaria *et al.*, Two-stage seeded soft-X-ray free-electron laser, Nat. Photonics **7**, 913 (2013).

[5] S. Di Mitri, M. Cornacchia, and S. Spampinati, Cancellation of Coherent Synchrotron Radiation Kicks with Optics Balance, Phys. Rev. Lett. **110**, 014801 (2013).

[6] H. Braun, F. Chautard, R. Corsini, T.O Raubenheimer, and P. Tenenbaum, Emittance Growth during Bunch Compression in the CTF-II, Phys. Rev. Lett. **84**, 658 (2000).

[7] J. Ellis and I. Wilson, Feature New physics with the Compact Linear Collider, Nature (London) **409**, 431 (2001).

[8] P. Emma, Reports No. SLAC-TN-05-004, No. LCLS-TN-01-1, 2001.

[9] Y. Sun, P. Emma, T. Raubenheimer, and J. Wu, X-band rf driven free electron laser driver with optics linearization, Phys. Rev. ST Accel. Beams **17**, 110703 (2014).

[10] S. Thorin, M. Eriksson, S. Werin, D. Angal-Kalinin, J. McKenzie, B. Militsyn, and P. Williams, in *Proceedings of the FEL2010, Malmö, Sweden* (Malmö, Sweden, 2010), WEPB34, p. 471.

[11] S. Di Mitri and M. Cornacchia, Electron beam brightness in linac drivers for free-electron-lasers, Phys. Rep. **539**, 1 (2014).

[12] K. L. F. Bane, Wakefields of sub-picosecond electron bunches, Int. J. Mod. Phys. A **22**, 3736 (2007).

[13] J. Arthur *et al.*, Linac Coherent Light Source Conceptual Design Report No. SLAC-R-593, 2002.

[14] B. Beutner, in *Proceedings of the 4th International Particle Accelerator Conference, IPAC-2013, Shanghai, China, 2013* (JACoW, Shanghai, China, 2013), WEPFI057, p. 2821.

[15] M. Cornacchia, P. Craievich, S. Di Mitri, G. Penco, M. Trovo, A. Zholents, P. Emma, Z. Huang, J. Wu, and D. Wang, in *Proceedings of the Future Light Source Work. FLS 2006* (2006), WG313, p. 3.

[16] Y. Kim, J. S. Oh, M. H. Cho, I. S. Ko, W. Namkung, D. Son, and Y. Kim, in *Proceedings of FEL2004 Conference* (Comitato Conferenze Elettra, Trieste, Italy, 2004), MOPOS18, p. 151.

[17] Y. Ding, K. L. F. Bane, W. Colocho, F. Decker, P. Emma, J. Frisch, M. W. Guetg, Z. Huang, R. Iverson, J. Krzywinski, H. Loos, A. Lutman, T. J. Maxwell, H. Nuhn, D. Ratner, J. Turner, J. Welch, and F. Zhou, Beam shaping to improve the free-electron laser performance at the Linac Coherent Light Source, Phys. Rev. Accel. Beams **19**, 100703 (2016).

[18] M. Borland, Simple method for particle tracking with coherent synchrotron radiation, Phys. Rev. ST Accel. Beams **4**, 070701 (2001).

[19] H. H. Braun, R. Corsini, L. Groening, F. Zhou, A. Kabel, T. O. Raubenheimer, R. Li, and T. Limberg, Emittance growth and energy loss due to coherent synchrotron radiation in a bunch compressor, Phys. Rev. ST Accel. Beams **3**, 124402 (2000).

[20] Y. S. Derbenev, J. Rossbach, E. L. Saldin, and V. D. Shiltsev, Report No. TESLA-FEL-95-05, 1995.

[21] M. Dohlus and T. Limberg, in *Proceedings of the 21st Particle Accelerator Conference, Knoxville, TN, 2005* (IEEE, Piscataway, NJ, 2005), p. 1015.

[22] R. Bonifacio, L. De Salvo, P. Pierini, N. Piovella, and C. Pellegrini, Spectrum, Temporal Structure, and Fluctuations in a High-Gain Free-Electron Laser Starting From Noise, Phys. Rev. Lett. **73**, 70 (1994).

[23] S. Di Mitri, Maximum brightness of linac-driven electron beams in the presence of collective effects, Phys. Rev. ST Accel. Beams **16**, 050701 (2013).

[24] S. Di Mitri, On the importance of electron beam brightness in high gain free electron lasers, Photonics **2**, 317 (2015).

[25] F. Zhou, K. Bane, Y. Ding, Z. Huang, H. Loos, and T. Raubenheimer, Measurements and analysis of a high-brightness electron beam collimated in a magnetic bunch compressor, Phys. Rev. ST Accel. Beams **18**, 050702 (2015).

[26] C. Mitchell, J. Qiang, and P. Emma, Longitudinal pulse shaping for the suppression of coherent synchrotron radiation-induced emittance growth, Phys. Rev. ST Accel. Beams **16**, 060703 (2013).

[27] F. Stulle, A. Adelmann, and M. Pedrozzi, EUROTeV-Report-2007-009, 2007.

[28] T. K. Charles, D. M. Paganin, and R. T. Dowd, Caustic-based approach to understanding bunching dynamics and current spike formation in particle bunches, Phys. Rev. Accel. Beams **19**, 104402 (2016).

[29] R. J. England, J. B. Rosenzweig, and G. Travish, Generation and Measurement of Relativistic Electron Bunches Characterized by a Linearly Ramped Current Profile, Phys. Rev. Lett. **100**, 214802 (2008).

[30] P. Piot, D. R. Douglas, and G. A. Krafft, Longitudinal phase space manipulation in energy recovering linac-driven free-electron lasers, Phys. Rev. ST Accel. Beams **6**, 030702 (2003).

[31] D. Douglas, Report No. JLAB-TN-98-025, 1998.

[32] M. Borland, Adv. Phot. Source Report No. LS-287, 2000.

[33] R. J. England, J. B. Rosenzweig, G. Andonian, P. Musumeci, G. Travish, and R. Yoder, Sextupole correction of the longitudinal transport of relativistic beams in dispersionless translating sections, Phys. Rev. ST Accel. Beams **8**, 012801 (2005).

[34] E. Vogal, M. Dohlus, H. Edwards, E. Harms, M. Huening, and K. Jensch, in *Proceedings of the SRF2007* (Peking University, Beijing, China, 2007), WEP17, pp. 481–485.

[35] W. Decking, G. Hoffstaetter, and T. Limberg, Report No. TESLA-2000-40, 2000.

[36] P. Emma, Reports No. DESY-TESLA-98-31, No. DAP-NIA-SEA-98-54, 1998.

[37] A. He, F. Willeke, L. H. Yu, L. Yang, T. Shaftan, G. Wang, Y. Li, Y. Hidaka, and J. Qiang, Design of low energy bunch compressors with space charge effects, Phys. Rev. ST Accel. Beams **18**, 014201 (2015).

[38] M. J. Boland, T. Charles, R. Dowd, G. S. Leblanc, Y. E. Tan, K. P. Wootton, D. Zhu, R. Corsini, A. Grudiev, A. Latina, D. Schulte, S. Stapnes, I. Syratchev, and W. Wuensch, in *Proceedings of the IPAC14, Dresden, Germany* (Dresden, Germany, 2014), THPME081.

[39] A. Aksoy, Ö. Yava, D. Schulte, A. Latina, W. Wuensch, A. Grudiev, I. Syratchev, Z. Nergiz, M. Jacewicz, R. Ruber, V. Ziemann, G. D'auria, S. Di Mitri, M. J. Boland, T. Charles, R. Dowd, G. LeBlanc, Q. Gu, and W. Fang, in *Proc. FEL2014, Basel, Switzerland*, MOP062 (Basel, Switzerland, 2014) pp. 3–6.

[40] Y. Sun, Second-order achromat design based on FODO cell, Phys. Rev. ST Accel. Beams **14**, 060703 (2011).

[41] B. E. Carlsten and T. O. Raubenheimer, Emittance growth of bunched beams in bends, Phys. Rev. E **51**, 1453 (1995).

[42] Y. S. Derbenev and V. D. Shiltsev, Report No. SLAC-PUB-7181, 1996.

[43] Y. Jing, Y. Hao, and V. N. Litvinenko, Compensating effect of the coherent synchrotron radiation in bunch compressors, Phys. Rev. ST Accel. Beams **16**, 060704 (2013).

[44] M. Dohlus, A. Kabel, and T. Limberg, in *Proceedings of the 18th Particle Accelerator Conference, New York, 1999* (IEEE, New York, 1999), TUP74, p. 1650.

[45] M. Dohlus, T. Limberg, and P. Emma, ICFA Beam Dyn. Newsl. No. 38 (2005).

[46] M. Borland, Y. Chae, and S. Milton, in *Proceedings of the 19th Particle Accelerator Conference, Chicago, IL, 2001* (IEEE, Piscataway, NJ, 2001), p. 2707.

[47] Z. Huang, M. Borland, P. Emma, J. Wu, C. Limborg, G. Stupakov, and J. Welch, Suppression of microbunching instability in the linac coherent light source, Phys. Rev. ST Accel. Beams **7**, 074401 (2004).

[48] T. Poston and I. Stewart, *Catastrophe Theory and Its Applications* (Dover Publications, New York, 1998), p. 512.

[49] M. V. Berry and C. Upstill, IV catastrophe optics: morphologies of caustics and their diffraction patterns, Prog. Opt. **18**, 257 (1980).